# The Mechanism of Rhodium Catalyzed Allylic C–H Amination

Robert J. Harris,[†] Jiyong Park,[‡,§] Taylor A. F. Nelson,[†] Nafees Iqbal,[‡,§] Daniel C. Salgueiro,[†] John Bacsa,[†] Cora E. MacBeth,[†] Mu-Hyun Baik*[,§,‡] and Simon B. Blakey*[,†]

[†]Department of Chemistry, Emory University, Atlanta, GA, 30322, U.S.A.

[‡]Department of Chemistry, Korea Advanced Institute of Science and Technology (KAIST), Daejeon 34141, Republic of Korea

[§]Center for Catalytic Hydrocarbon Functionalizations, Institute for Basic Science (IBS), Daejeon 34141, Republic of Korea

**ABSTRACT**

Herein the mechanism of catalytic allylic C–H amination reactions promoted by Cp*Rh complexes is reported. Reaction kinetics experiments, stoichiometric studies, and DFT calculations demonstrate that the allylic C–H activation to generate a Cp*Rh(π-allyl) complex is viable under mild reaction conditions. The role of external oxidants in the catalytic cycle is elucidated. Quantum mechanical calculations, stoichiometric reactions, and cyclic voltammetry experiments concomitantly support an oxidatively induced reductive elimination process of the allyl fragment with an acetate ligand proceeding through a Rh(IV) intermediate. Stoichiometric oxidation and bulk electrolysis of the proposed π-allyl intermediate are also reported to support these analyses. Lastly, evidence supporting the amination of an allylic acetate intermediate is presented. We show that $Cp^*Rh(III)^{2+}$ behaves as a Lewis acid catalyst to complete the allylic amination reaction.

**Keywords:** Density Functional Theory, C–H amination, Rhodium, Allylic functionalization, Mechanism

## INTRODUCTION

Transition-metal-mediated direct activation of C($sp^3$)–H bonds to install C–X (X = C, N, and O) functionalities has become an indispensable method in modern synthetic strategy. Precisely controlling the regio- and diastereoselectivities in these reactions is a key challenge that has been achieved using directing groups[1] or by taking advantage of the inherent reactivities of the C–H bonds.[2] Direct and efficient synthetic protocols that afford desired selectivities continue to be actively sought after. For many years, palladium catalyzed C–H allylic functionalization has been studied with simple olefins.[3] In 2004, White and co-workers reported the catalytic allylic C–H acetoxylation of terminal olefins in complex settings catalyzed by palladium.[4] In a series of reports that followed, Pd(π-allyl) intermediates were intercepted with a variety of stabilized carbon, nitrogen, and oxygen nucleophiles (Scheme 1A).[5] Cossy and co-workers subsequently reported the use of a Cp*Rh precatalyst to catalyze the intramolecular cyclization of aminoalkenes by allylic C–H functionalization, as illustrated in Scheme 1B.[6] More recently our group disclosed the intermolecular allylic C–H amination of internal olefins with primary and secondary amines bearing only one electron withdrawing group (Scheme 1C).[7] This foundational study paved the way for additional rhodium and iridium catalyzed allylic C–H functionalization protocols, including etherification, arylation, and amidation reactions.[8]

**Scheme 1.** Transition metal catalyzed allylic C–H amination

A) Allylic C–H Functionalization of Terminal Olefins
(White 2004 - 2018)

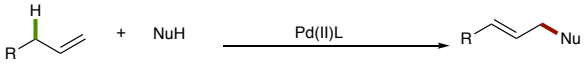


NuH = $RCO_2H$, $CH_2(EWG)_2$, $TsNH(CO_2Me)$, $TfNH_2$

B) Intramolecular Allylic C–H Functionalization Using RhCp*
(Cossy 2012)

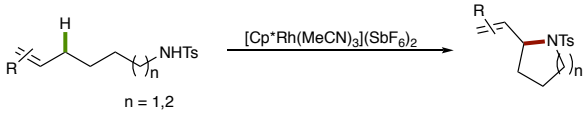


n = 1,2

C) Intermolecular Allylic C–H Functionalization of Internal Olefins
(Blakey 2017)

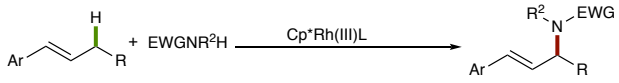


The development of catalytic methods for C($sp^3$)–H functionalization has exceeded our mechanistic understanding of these transformations. In the case of rhodium catalyzed allylic C–H functionalization, Cossy suggested that a plausible mechanism would involve an allylic C–H insertion to generate a Rh(π–allyl) complex followed by *N*–metallation and reductive elimination from a Rh(III)

intermediate to generate the allylic amine and a Rh(I) species that would be reoxidized to Rh(III) to complete the catalytic cycle (see supplemental Scheme S1). The proposed mechanism is in accord with reports on the rhodium catalyzed allylic substitution with phosphine and phosphite supporting ligands.[9] Similar catalytic reactions involving Rh(III/I) have also been proposed for C($sp^2$)–H bond activations that utilize cyclopentadienyl supporting ligands.[10] However, we note that higher oxidation states of rhodium have also been proposed in Cp*Rh catalyzed C($sp^2$)–H activation.[11]

Providing additional complexity to the mechanistic picture, the synthesis and reactivity of several group IX π–allyl complexes similar to those invoked by Cossy and our group in the Cp*Rh catalyzed allylic C–H amination have been reported. Bergman isolated and characterized the Cp*Rh(π–allyl) complex **I** (Figure 1A)[12] and Stryker subsequently determined the structures of the *exo* and *endo* isomers of IrCp*(π–allyl) complex **II** (Figure 1B).[13] In each case, the *exo*–isomers of the π–allyl complexes react with hard nucleophiles at the central carbon to generate metallocyclobutane products. Additionally, Tanaka reported the isolation and characterization of the $Cp^E$Rh(III)(π–allyl) complex **III** bearing a pendent tosyl amine nucleophile (Figure 1C) ($Cp^E$ = 1,3-diethylester-2,4,5-trimethylcyclopentadiene, see Figure 1C).[14] When complex **III** was treated with $AgSbF_6$ to abstract the chloride and generate a vacant coordination site for *N*–metallation, the expected cyclization product was not observed. When complex **III** was treated with both $AgSbF_6$ and $Cu(OAc)_2$, the expected amination product was observed in 51% yield. The authors did not postulate specific roles of $Cu(OAc)_2$ in this transformation. However, Jones and coworkers have reported the use of a copper salt as an oxidant to induce reductive elimination of a C($sp^2$)–N($sp^2$) bond from a Cp*Rh(III) complex.[11b] In 2017, Chang and Baik reported a detailed mechanistic study of a C–H arylation reaction catalyzed by Cp*Ir, in which a strong oxidant facilitates the C–H arylation by oxidizing the metalated complex via an oxidatively induced reductive elimination (Figure 1D).[15] The reactivities of **III** are largely inconsistent with the previously proposed Rh(III/I) mechanism for Cp*Rh catalyzed allylic C–H amination.

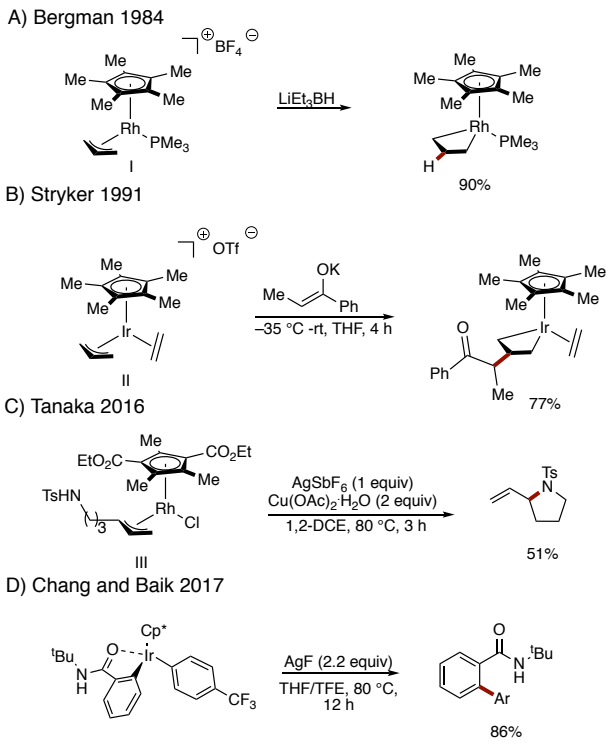


**Figure 1.** Previously reported reactions of group IX π–allyl complexes

Herein, we describe a detailed mechanistic study of allylic C–H aminations via a Cp*Rh(III)(π-allyl) intermediate, combining experimental observations including kinetic analysis, isolation and subsequent characterizations of putative intermediates and their reactivities. These experimental findings were corroborated with cyclic voltammetry measurements and quantum mechanical calculations, to elucidate the mechanistic details of the Rh-catalyzed C($sp^3$)–H activations that afford allylic amination products.

## RESULTS AND DISCUSSION

### Kinetic Analysis

To obtain experimental data to facilitate a deeper understanding of the mechanism for the rhodium catalyzed allylic C–H amination, we targeted 1,3-diphenylpropene **1** as a simple model substrate, in which complications caused by regioselectivity are not present (Scheme 2). We note that our initial attempt to monitor the reaction progress using *p*-toluenesulfonamide as a nucleophile was complicated due to its insolubility, leading us to choose benzyl carbamate as the nucleophile.

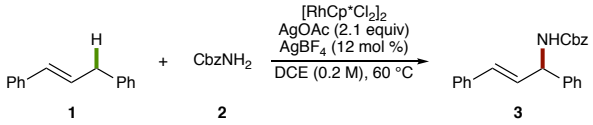


**Scheme 2.** Reaction scheme for allylic C–H amination for kinetic analysis

Analysis of initial rates of reactions of diphenylpropene **1** with carbamate **2** catalyzed by $[Cp^*RhCl_2]_2/AgBF_4$ showed that allylic amine production was linearly dependent on the concentrations of the Rh, alkene, and 1/carbamate with slopes of $k_1 = 2.4 \pm 0.4 \times 10^{-4}$ s$^{-1}$, $k_2 = 1.5 \pm 0.1 \times 10^{-5}$ s$^{-1}$ and $k_3 = 1.4 \pm 0.2 \times 10^{-6}$ M$^2$ s$^{-1}$ respectively (Figures S1-S6). These data indicate the reaction is first-order in rhodium and alkene concentrations. Also, an inverse rate constant for the carbamate concentration was observed, that is consistent with the carbamate nucleophile binding to the rhodium catalyst in an off–cycle equilibrium (Scheme S2).

Kinetic isotope experiments provide insight into the rate determining step (RDS). A 1:1 mixture of **1** and **1**–$d_2$ (0.2 M) in DCE was treated with carbamate **2** (0.49 M), $[Cp^*RhCl_2]_2$ ([Rh] = 12 mM), $AgBF_4$ (26 mM), and AgOAc (2.1 equiv). The reaction was stopped after 2 hours (~10% conversion), and allylic amine **3** was isolated in 5% yield (Figure 2). Analysis of the $^1$H NMR of **3** established deuterium incorporation in 28 % of the product, with the label observed equally at both C1 and C3. This observation is consistent with a primary KIE of $k_H/k_D = 2.6$, and the intermediacy of a symmetrical π-allyl complex. In our original disclosure of the rhodium catalyzed allylic C–H amination, we showed that C–H cleavage was irreversible.[7] Taken together, these observations along with the first order dependence of rate on **1**, establish that C–H cleavage is rate-determining.[16]

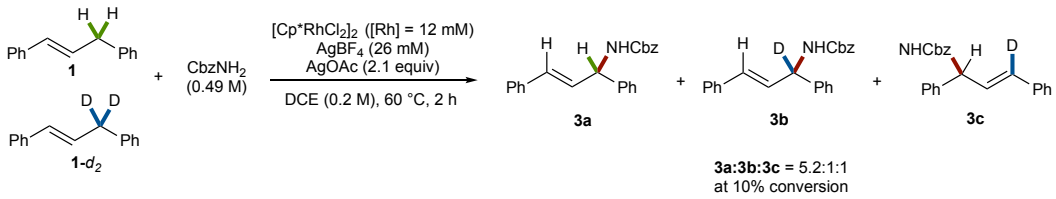


**Figure 2.** Amination of a 1:1 mixture of **1** and **1**–$d_2$ with benzyl carbamate catalyzed by $[Cp^*RhCl_2]_2$

## Synthesis, Characterization, and Reactivity of Rhodium π-allyl Complexes

The kinetic data presented above are consistent with the notion that C–H activation is rate limiting. Consequently, overall reaction kinetics cannot be used to probe the mechanism of C–N bond formation

or catalyst regeneration. In order to gain insight into this sequence in the catalytic cycle, we synthesized plausible intermediates in the catalytic cycle and examined their reactivities. Analogous to Tanaka's synthesis of $Cp^{E}Rh(\pi\text{–allyl})$ complex **III**, we attempted to synthesize a Rh(π–allyl) complex with a Cp* supporting ligand. Initial attempts to make a Cp*Rh(π–allyl) complex starting from $[Cp^*RhCl_2]_2$ in the presence of $AgSbF_6$ were unsuccessful and led to a complex mixture of products. However, stirring $[Cp^*Rh(MeCN)_3](SbF_6)_2$ with cesium acetate (1.5 equiv) and 4-phenyl-1-butene (2 equiv) in DCM at room temperature for 16 h followed by the addition of tetraethylammonium chloride, led to the isolation of a mixture of Rh(π–allyl) complexes **IV** and **V** in 53% yield (9:1 ratio, Figure 3A). By using 1,2–DCE as a solvent and heating the reaction to 80 °C we were able to isolate complex **V** exclusively as the thermodynamic product in 61% yield (Figure 3B).

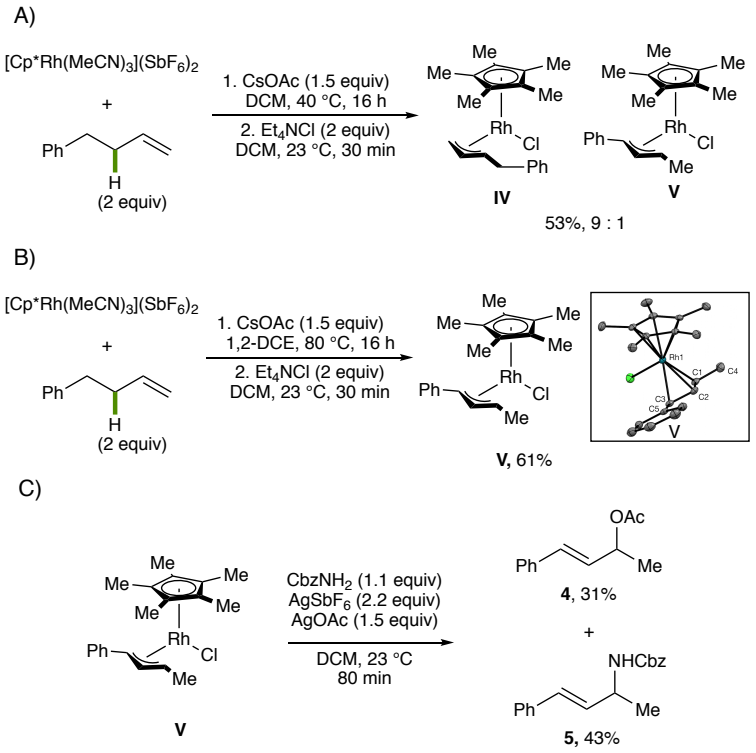


**Figure 3.** Synthesis and structure of Cp*Rh(π–allyl)Cl complex. A) Synthesis of a mixture of internal (**IV**) and terminal (**V**) RhCp*(π-allyl) complexes. B) Synthesis for selectively forming the terminal Cp*Rh(π-allyl)Cl complex **V**. C) Stoichiometric reactivity of complex **V** in catalytic reaction conditions. ORTEP diagram of **V** depicted with ellipsoids shown at the 50% probability level and hydrogen atoms omitted for clarity

Complex **V** was fully characterized by $^{1}H$ and $^{13}C$ NMR spectroscopy and single crystal X-ray diffraction. The $^{1}H$ NMR spectrum of **V** displayed a characteristic triplet of doublets at $\delta = 4.55$ ppm with coupling constants $J_{HH} = 10.7$ Hz and $J_{RhH} = 2.0$ Hz corresponding to the proton attached to the central carbon of the π-allyl ligand. Vapor diffusion of pentane into a concentrated ether solution of **V** at 25 °C

provided crystals suitable for X-ray analysis (Figure 3B, inset). The allyl ligand of complex **V** adopts a near planar geometry with dihedral angles C1–C2–C3–C5 = 173.8° and C4–C1–C2–C3 = 178.6°. The Rh–C1 and Rh–C3 bond distances are approximately equal with bond lengths of 2.203(2)Å and 2.219(2)Å, respectively, while the Rh–C2 bond length is significantly shorter with a bond length of 2.133(2) Å.

With complex **V** in hand, we began to investigate the reactivities of Cp*Rh(π-allyl) complexes towards nucleophiles. In an initial experiment, complex **V** was treated with a single equivalent of carbamate **2** in DCM at 23 °C. Unsurprisingly, even after 48 h, complex **V** remained unreacted. However, when complex **V** was treated with benzylcarbamate (**2**, 1.1 equiv) in the presence of $AgSbF_6$ (2.2 equiv, as a halide abstractor) and AgOAc (1.5 equiv) in DCM at 23 °C to mimic the reaction conditions that yielded aminated products, both allylic acetate **4** and the expected allylic amine **5** were generated in 31% and 43% yield respectively (Figure 3C). This result suggests that while **V** is likely not a catalytically relevant species, the cationic complex generated from abstracting a chloride from **V** could be. Also, this result indicated that silver additives are essential for the activation of the Rh(π-allyl) complex **V**. Lastly, the significant quantities of allylic acetate **4** observed in the reaction lead us to consider the possibility that the amination reaction might proceed through an allylic acetate intermediate.

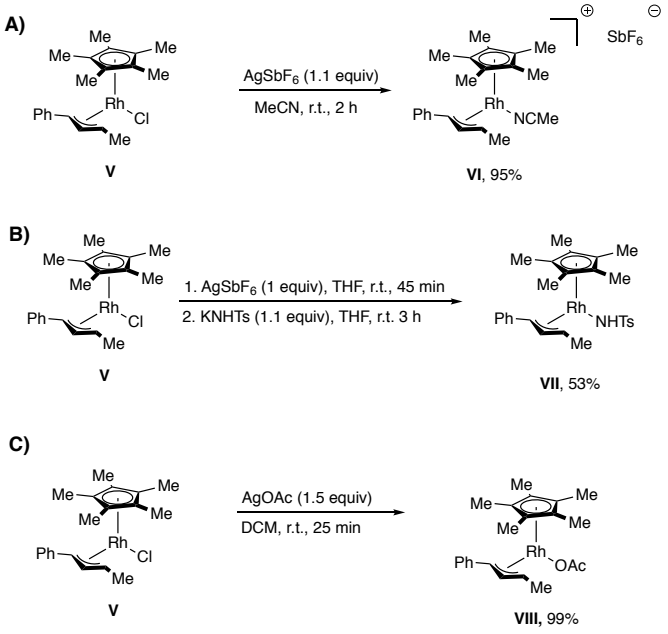


**Figure 4.** Synthesis of Cp*Rh(III)(π-allyl) complexes bearing A) acetonitrile, B) tosyl amine, and C) acetate ligands

To further probe these possibilities, we synthesized the cationic [Cp*Rh(π–allyl)(MeCN)]($SbF_6$) complex **VI** (Figure 4A), the Cp*Rh(π–allyl)(NHTs) complex **VII** (Figure 4B) and the Cp*Rh(π–

allyl)(OAc) complex **VIII** (Figure 4C). Complexes **VI**, **VII** and **VIII** were characterized by $^{1}H$ and $^{13}C$ NMR spectroscopy and single crystal X-ray diffraction (see supplemental for full XRD data). Dichloroethane solutions of complex **VII** and complex **VIII** were heated to 60 °C and both compounds were stable over a 6-hour period. The isolation and stability of complexes **VII** and **VIII** unambiguously rules out the possibility that allylic C–N or C–O bond formation by reductive elimination from these Rh(III) species is possible under the catalytic conditions. Furthermore, the fact that no allylic amine or allylic acetate product was observed during the synthesis of complexes suggests that outer-sphere nucleophilic attack of these nucleophiles on cationic Rh(III)(π–allyl) complexes is not a plausible explanation for product formation in the catalytic reaction.

This conclusion is further supported by the observation that no allylic amine was observed, even after cationic complex **VI** was reacted with benzylcarbamate at 40°C for 14 h. Instead, Cp*Rh(π–allyl)Cl complex **V** was recovered in 92% yield after a chloride quench (Figure 5A). To investigate the potential for an oxidatively induced reductive elimination mechanism to be operating, we exposed both Cp*Rh(π–allyl)(NHTs) complex **VII** and Cp*Rh(π–allyl)(OAc) complex **VIII** to two equivalents $AgSbF_6$. In the reaction of Cp*Rh(π–allyl)(NHTs) complex **VII**, two equivalents of benzenesulfonamide were included allowing us to probe both an oxidatively induced inner-sphere reductive elimination, and an oxidatively induced outer-sphere nucleophilic attack. In this reaction, only 10% combined yield of allylic amine products (**6** and **7**) was observed. No rhodium(π-allyl) complexes could be recovered (Figure 5B). In contrast, when the Cp*Rh(π-allyl)(OAc) complex **VIII** was oxidized with two equivalents $AgSbF_6$, clean conversion to the allylic acetate product **4** was observed (Figure 5C). These observations suggest that the catalytic allylic amination reaction proceeds through an allylic acetate intermediate, obtained by an oxidatively induced reductive elimination mechanism.

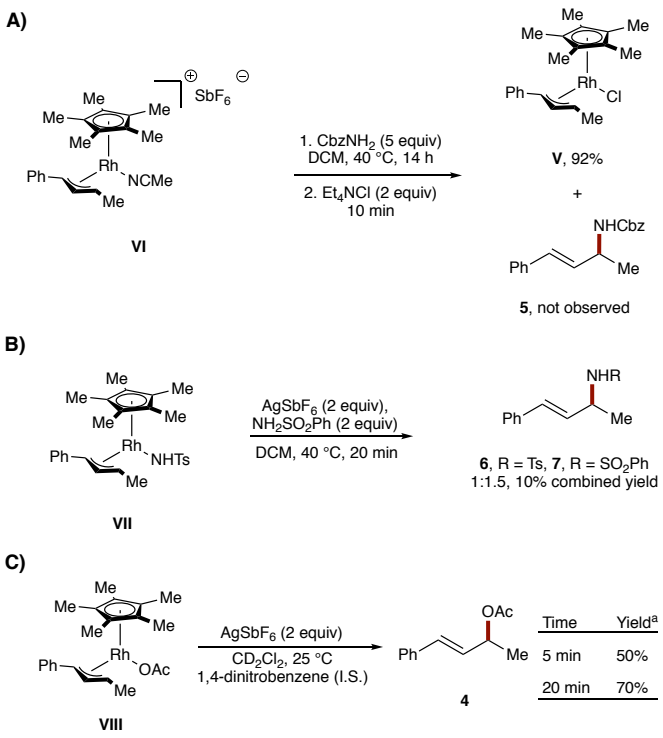


**Figure 5.** Reactivity of Cp*Rh(III)(π-allyl) complexes demonstrating the feasibility of oxidatively induced reductive elimination of an allyl acetate. A) Reaction scheme of benzyl carbamate reactivity with complex **VI**.B) Reaction scheme of benzene sulfonamide with complex **VII**. C) Reaction scheme of complex **VIII** with $AgSbF_6$ as an oxidant resulting in clean conversion to acetate **4**. *a* Yields were determined by $^1H$ NMR analysis of the reaction mixture using 1,4-dinitrobenzene as an internal standard.

To complete our experimental investigation, we demonstrated that allylic acetate **4** is readily converted to allylic amine **5** in the presence of the Lewis acid components present in the catalytic reactions (Table 1). Both $AgSbF_6$ and $AgBF_4$ were found to be competent Lewis acid catalysts providing product in 91% and 76% yield, respectively. We also confirmed that $[Cp^*Rh(MeCN)_3](SbF_6)_2$ and $(Cp^*RhCl_2)_2$ are competent Lewis acid catalysts after halide abstraction, affording **5** in at 73 % and 84 %, respectively. In the absence of either silver cation or Cp*Rh, the allylic acetate remained unchanged. We note that the Ag(I) and Cp*Rh(III) catalyzed allylic amination of allylic acetate **8** proceeds readily even at reduced temperatures (Table 1, entry 6 to 8). Time course studies of Ag(I) and Cp*Rh(III) also provided insight into the relative rates of catalysis (Figures S11-S12). We noted that at 0 ºC Ag(I) catalysis proceeded to completion in 2.5 h, while Cp*Rh(III) proceeded to completion in seconds. These data strongly supported a plausible mechanistic hypothesis toward the completion of the allylic amination catalytic cycle via Cp*Rh(III) catalyzed allylic substitution which will be discussed further.

**Table 1.** Reactivity of allylic acetate and benzyl carbamate in the presence of Ag(I) or Rh(III) as a catalyst.

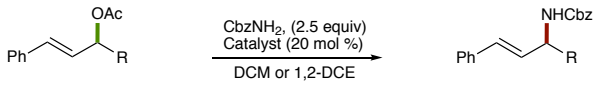


| entry | Time | R | Temp (ºC) | Catalyst | Yield |
|---|---|---|---|---|---|
| 1 | 3 h | Me | 60 | $AgSbF_6$ | 91%[a] |
| 2 | 3 h | Me | 60 | $AgBF_4$ | 76%[a] |
| 3 | 3 h | Me | 60 | $[Cp^*RhCl_2]_2/AgSbF_6$[c] | 73%[a] |
| 4 | 3 h | Me | 60 | $[Cp^*Rh(MeCN)_3](SbF_6)_2$ | 84%[a] |
| 5 | 3 h | Me | 60 | none | 0%[a,d] |
| 6 | 5 min | Ph | 0 | $[Cp^*Rh(MeCN)_3](SbF_6)_2$ | 97%[b] |
| 7 | 5 min | Ph | 0 | $AgSbF_6$ | 47%[b] |
| 8 | 2.5 h | Ph | 0 | $AgSbF_6$ | 90%[b] |

[a]Reactions were performed in 1,2-DCE and yield determined by crude reaction analysis by proton $^1$H NMR against 1,4-dinitrobenzene. [b]Reactions were performed in DCM and yield determined by GC analysis against nonane as internal standard (see supplemental for full time course) [c]$[Cp^*RhCl_2]_2$ (25 mM) and $AgSbF_6$ (40 mM) were stirred in DCM with benzyl carbamate (**2**) at 60 °C for 30 min before allylic acetate **4** was added to be sure that there was no $Ag^+$ in solution. [d]Allylic amine was not observed by $^1$H NMR.

## Computational Investigation of the Key Steps in the Catalytic Cycle

Density functional theory (DFT) calculations were carried out to construct a catalytic mechanism incorporating the experimental observations mentioned above. Using 1,3-diphenylpropene as the substrate, we compared the activation barriers of the reductive elimination from the three relevant oxidation states Rh(III), Rh(IV) and Rh(V), as illustrated in Figure 6. The reductive elimination initiated from the Rh(III) intermediate to give Rh(I) is not viable, as the computed activation barrier of 38.4 kcal/mol corresponds to an Eyring rate of $4.8\times10^{10}$/s or equivalently $0.7\times10^{-8}$ mol/day at 313 K (Figure 6a). As expected, the oxidation of the metal center to Rh(IV) lowers the activation barrier notably by more than 21 kcal/mol to 17.6 kcal/mol (Figure 6b), which suggests an acceleration of the reaction by more than $10^{10}$ fold compared to the Rh(III) intermediate. Our calculations suggest that a second oxidation to access the Rh(V) center does not enhance the reaction rate further, as the calculated barrier increases to 19.5 kcal/mol (Figure 6c).

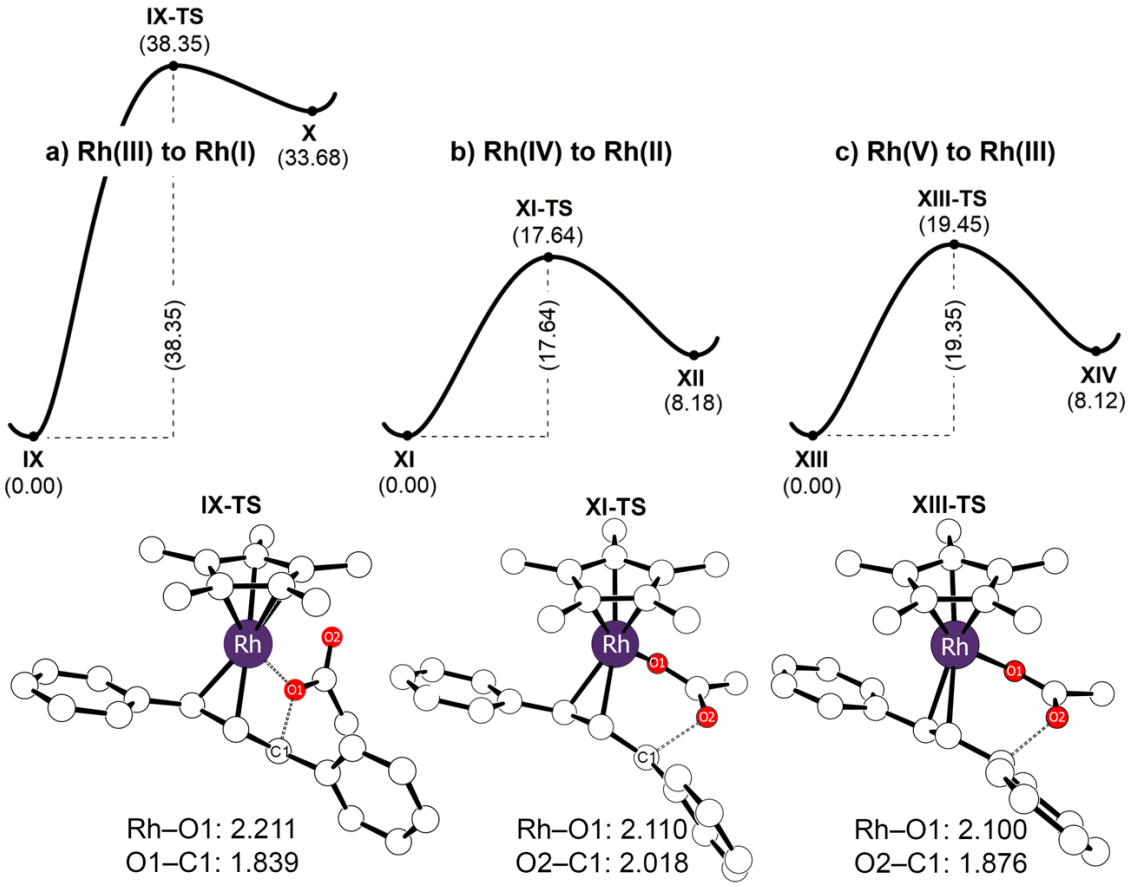


**Figure 6.** Calculated energy profiles for reductive elimination from the a) Rh(III)–, b) Rh(IV)–, and c) Rh(V)–π-allyl intermediates, leading to the Rh(I), Rh(II), and Rh(III) products, respectively. The detailed molecular structure of each TS is shown as well. The unit of energy is kcal/mol and of bond length is Å.

A closer inspection of the transition structures reveals that the two oxygen atoms of the acetate introduce a slight variation in the transition states. During the reductive elimination from the Rh(III)–center, the C–O bond is formed by the acetate–oxygen that is directly bound to the metal, as illustrated in Figure 6a. The Rh–O bond elongates from 2.121 to 2.211 Å as the transition state **IX-TS** is traversed with the C–O distance being 1.839 Å. This bond forming event is best conceptualized by considering that the allylic fragment formally donates two electrons to the Rh-center to accomplish the reductive part of the reductive elimination step. Consequently, it becomes a positively polarized electrophile that can engage the acetate and form the C–O bond. Of course, these two processes are concerted in reality, but it is instructive to visualize them separately. When the metal is oxidized to Rh(IV) or Rh(V), it is the distal oxygen of the acetate that attacks the allylic carbon and the Rh–O bond is mostly maintained with the Rh–O bond lengths being 2.110 (**XI-TS**) and 2.100 Å (**XIII-TS**), respectively, as illustrated in Figures 6b and 6c. On the contrary, reductive coupling of the oxygen atom bonded to the metal center is energetically

less favorable, for the oxidized metal centers (Rh(IV) and Rh(V)). When traversing the Rh(IV)-Rh(II) cycle, the activation barrier is elevated to 24.9 kcal/mol (**XI-TS'** in Figure S15) and for the Rh(V)-Rh(III) cycle, the corresponding barrier is 22.6 kcal/mol (**XIII-TS'** in Figure S15). Thus, whereas the Rh(III) center carries out a classical reductive elimination, the other higher valent metal centers prefer to reductively couple the acetate with the allyl functionality without eliminating the acetate. This subtle change in mechanism is easy to understand considering that the Rh–O bond becomes much stronger in Rh(IV) and Rh(V) compared to Rh(III). As the acetate acts as a nucleophile in this step, the higher oxidation state at the metal decreases its nucleophilicity and results in a higher barrier in the Rh(V)-complex. Thus, Rh(IV) constitutes an ideal compromise between the two governing forces, namely the ability of the metal center to oxidize the allyl fragment and the nucleophilicity of the acetate.

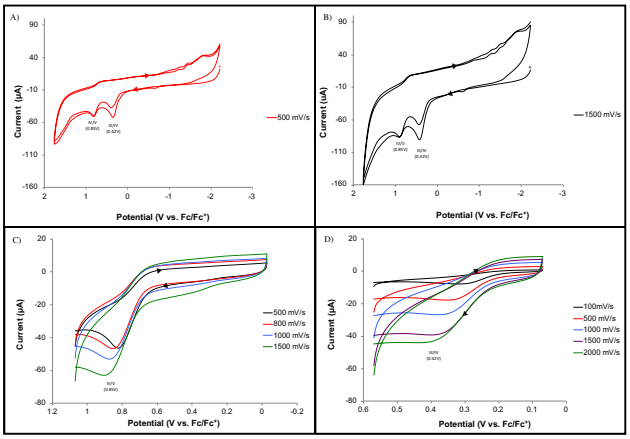


**Figure 7.** Cyclic voltammogram of **VIII** recorded at room temperature in DCM (0.001 M in 0.10 M *n*-$Bu_4NPF_6$). A) Full scan width cyclic voltammagram from 1.7 V to -2.2 V recorded at 500 mV/s. B) Full scan width cyclic voltammagram from 1.7 to -2.2 V recorded at 1500 mV/s. C) Voltammograms for proposed Rh(IV/V) couple recorded at 500 mV/s, 800 mv/s, 1000 mV/s, and 1500 mV/s) D) Voltammograms for proposed Rh(III/IV) couple recorded at 100 mV/s, 500 mV/s, 1000 mV/s, 1500 mV/s, and 2000 mV/s. See supplemental figure S13 for additional electrochemical details.

To test the proposed catalytic mechanism, cyclic voltammetry experiments were carried out to investigate the redox profile of **VIII**. Complex **VIII** showed two irreversible oxidation events, suggesting that both Rh(IV) and Rh(V) are thermodynamically accessible on an electrochemical time scale (Figure 7A and 7B). As is expected for an electrochemical step that is coupled with a chemical event, the peak positions of both steps are scan rate dependent (Figures 7C and 7D). The first oxidation occurs at $E_1$ = ~0.42 V versus $Fc/Fc^+$ which we assign to the Rh(III)/(IV) couple, and the second event occurs at $E_2$ = ~0.85 V which we attributed to the Rh(IV)/(V) couple. These data are consistent with an electrochemical

process coupled to a chemical event, and support our hypothesis that reductive elimination takes place from the Rh(IV) intermediate. Additionally, we note that the redox potential of $Ag^+$ in DCM is ~0.65 V (AgTFA),[17] rendering it unlikely that the Rh(V) complex ($E_2$ = ~0.85 V) can be accessed using $Ag^+$ as an oxidant. Taken together, these data support a catalytic cycle that consists of a Rh(III) → Rh(IV) → Rh(II) → Rh(III) redox sequence. To further support these conclusions, we sought to investigate stoichiometric oxidation of **VIII** using an outer sphere oxidant closely matched to the Rh(III/IV) oxidation potential determined by cyclic voltammetry (i.e > ~0.42V). To this end, the stoichiometric oxidation of **VIII** utilizing 1,1'-diacetylferrocenium hexafluorophosphate ($E_{1/2}$ = +0.49V vs $Fc/Fc^+$)[17b] resulted in a 25% yield of the expected allylic acetate (Figure 8).

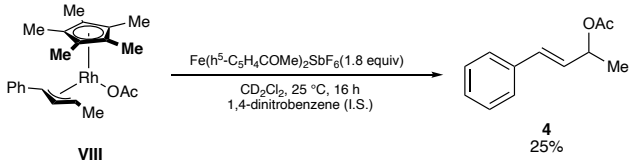


**Figure 8.** Stoichiometric oxidation of complex **VIII** with 1,1'-diacetylferrocenium hexafluorophosphate.

Scheme 3 summarizes the proposed mechanism of the Rh catalyzed allylic acetoxylation and Figure 9 shows the corresponding reaction energy profile. The catalytic cycle begins with the coordination of the acetate and the olefin substrates **1** to the Cp*Rh fragment to form the initial reactant complex **XV**, which undergoes a concerted metalation deprotonation (CMD) traversing the transition **XV-TS** to activate the allylic C–H bond. The computed activation energy for this step is 26.7 kcal/mol, which is in good agreement with the experimental observation that a mildly elevated temperature is required to prepare the acetate intermediate **VIII** (*vide supra*). Ligand exchange affords the Cp*Rh(III)(π-allyl)OAc complex **XI** from **XVI**. As discussed above, the reductive elimination from this intermediate is associated with a very high barrier (Figure 6a). To push the reaction forward, one electron oxidation of Rh(III) to Rh(IV) is needed which enables the reductive elimination via **XI-TS** with a computed barrier of 17.6 kcal/mol. Intermediate **XII** can easily undergo a one-electron oxidation to form the Rh(III) intermediate **XVII**, which releases product **8** via ligand exchange steps.

**Scheme 3.** Proposed catalytic mechanism of the rhodium catalyzed allylic acetoxylation going through Rh(IV)→Rh(II)

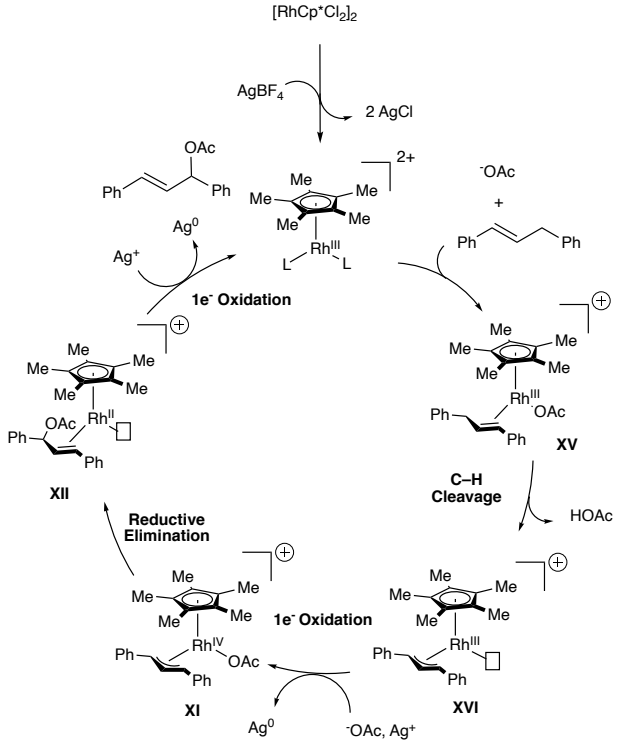


We also constructed the energy profile of inner-sphere amination initiated from Cp*Rh(IV)(π–allyl)OAc complex **XI**, that is also shown in Figure 9. The coordination of the rhodium center by a carbamate (**XIX**) is followed by the deprotonation of the amine by the pendant acetate, whose activation barrier is 20.6 kcal/mol (**XIX-TS**). Starting from the activated amine (**XX**), a reductive elimination step engages an allylic carbon and the pendant amine (**XX-TS**), that demands a computed activation energy barrier of 25.0 kcal/mol. The barrier for the amination is 7.4 kcal/mol higher in energy than that of the reductive elimination step affording the allylic acetate intermediate (**XI-TS**). The energy profile of the inner-sphere amination clearly shows that the kinetics of amination is much slower in progression than that of the acetoxylation. The computational finding is in good agreement with our experimental observation that the amination initiated from Cp*Rh(III)(π-allyl)TsNH (Figure 5b) yields lower conversion (10%) than that of the acetoxylation (Figure 5c), even though the temperature of amination reaction was higher. With the experimental and computational findings, we concluded there is a secondary catalytic cycle that converts initially formed allylic acetate **8** to the aminated product.

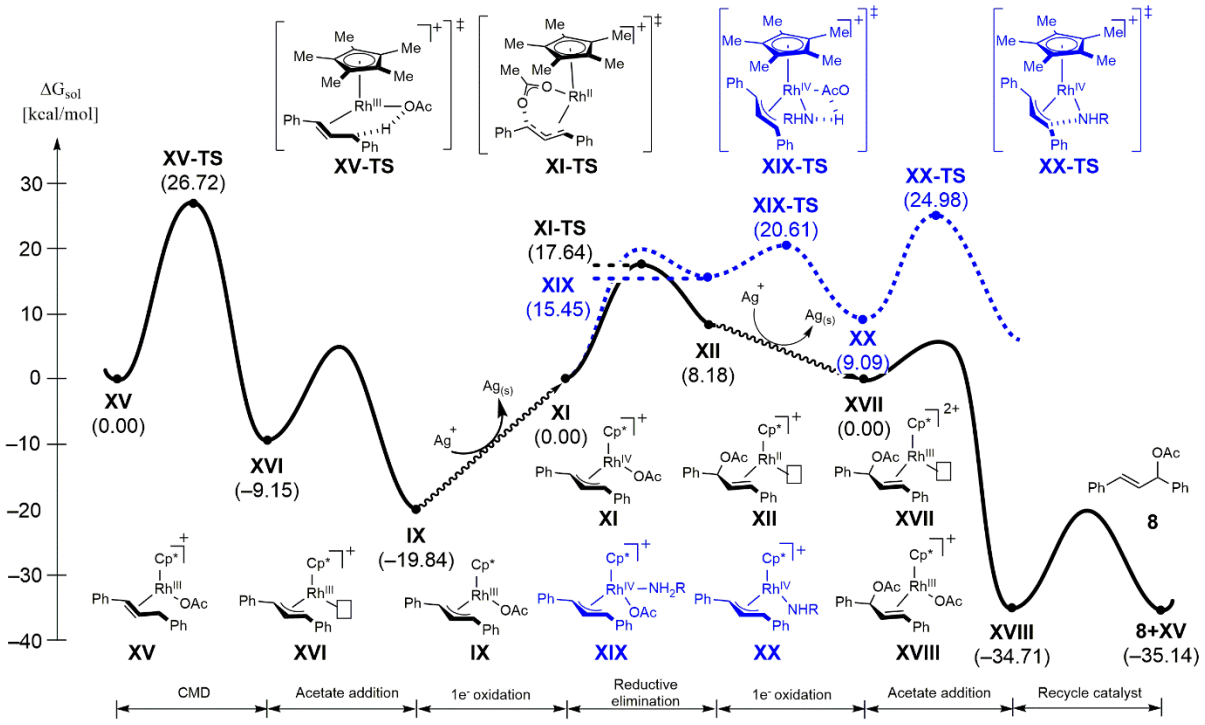


**Figure 9.** Energy profile for Rh-catalyzed allylic acetoxylation going through Rh (IV→II)

## Formation of Allylic Amines

With the detailed mechanism of the intermediate allylic acetate formation in hand, we turned our attention to the role of the silver and rhodium salts in the conversion of the allylic acetate to the allylic amine product. Based on the experimental findings that the amination is viable in the presence of Lewis acid components (Table 1), we hypothesized both Rh(III) and Ag(I) may serve as Lewis acid–catalysts promoting the nucleophilic substitution. In the following, we delineate the mechanistic details of the two possible mechanistic hypotheses for the formation of allylic amine product from the allylic acetate intermediate, by means of DFT calculations. Inspired by the related $AgSbF_6$ and $[Cp^*Rh(MeCN)_3](SbF_6)_2$ catalyzed amination of allylic acetate,[18] we compiled a plausible mechanistic pathway for the amination reaction which involves an initial $Ag^+$ or Cp* $Rh(III)^{2+}$ addition to allylic acetate to prepare Lewis acid coordinated allylic acetate complexes, as illustrated in Scheme 4 (scheme 4 shows the postulated cycle for Rh(III)). The corresponding energy profiles for the allylic amination of allylic acetate **8** are depicted in Figure 10. The catalytic cycle is initiated by the addition of the Lewis acid to the allylic acetate **8** yielding **9** or **10**. Out of the three possible scenarios of the nucleophilic substitutions ($S_N1$, $S_N2$, and $S_N2'$), our DFT calculations suggested that the $S_N1$ mechanism is the most plausible route for the nucleophilic substitution. The dissociation of MOAc (M = Ag or Rh) yield allylic cation intermediates **9a** and **10a**, associated with

an activation barrier of 14.4 kcal/mol (**9-TS**) and 14.8 kcal/mol (**10-TS**). The addition of amine nucleophiles (**9a-TS**)**/(10a-TS)** requires 16.7 kcal/mol of activation energy for the silver and 15.6 kcal/mol for the rhodium, which is predicted to be the most difficult step to activate of the amination reaction yet is viable under the reaction conditions tested. The difference in the activation barriers is in line with the observation that the amination is faster with Cp*Rh(III) than with Ag(I) (Figure S11-S12). To push the reaction forward, the aminated intermediates **9b/10b** undergo concerted deprotonations via traversing the transition structure **9b-TS/10b-TS** to produce the allylic amine product bound to the silver cation **9c** and to the Cp*Rh(III) **10c**. These data as well as our experimental results (Table 1) support that both silver cation ($Ag^+$) and Cp*Rh(III) acts as Lewis acids mediating the allylic substitution from allylic acetate **8** resulting in allylic amine **11**. A full reaction time course study (Figure S14) was conducted and is consistent with our proposed mechanism. A small, but measurable, steady state concentration of the allylic acetate (**8**) is observed over the course of the reaction. The small concentration of acetate **8** reflects the low calculated barrier for the substitution reaction (14.8 kcal/mol) compared to the turnover limiting C–H functionalization step (26.7 kcal/mol).

**Scheme 4.** Proposed mechanism for Lewis Acid Catalyzed Allylic Amination Reaction from Allylic Acetate

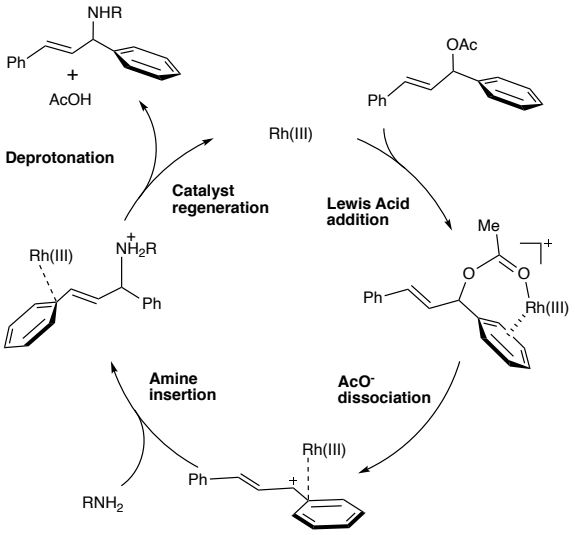

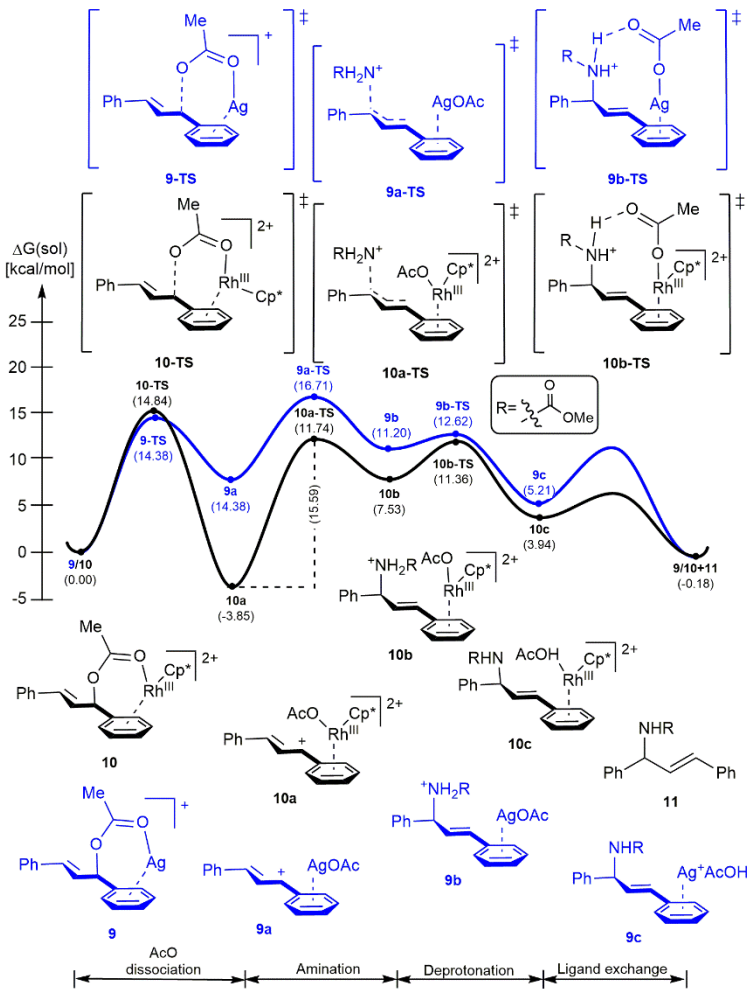


**Figure 10.** Energy profile for $AgSbF_6$ and $[Cp^*Rh(MeCN)_3](SbF_6)_2$ catalyzed allylic amination from allylic acetate. The Gibbs free energies were computed at 298.15 K.

## CONCLUSIONS

The computational and experimental data provided a detailed picture of the rhodium-catalyzed C($sp^3$)–H allylic amination. Overall, the rate-determining step of the entire catalytic cycles examined computationally was found to be the C–H activation of allylic substrate with a DFT-computed barrier of 26.8 kcal/mol. This is consistent with the experimental kinetic observations that also support C–H activation as the rate determining step in this transformation. Calculations revealed that the Rh catalyst facilitates the formation of the allylic acetate using the silver salt as an oxidizing agent via an oxidatively induced reductive elimination reaction[15] where the Rh(III) center of the key intermediate is first oxidized to Rh(IV). Interestingly, the two-electron oxidation to access the Rh(V) analogue is not found to accelerate the reaction and we report strong experimental evidence that Rh(IV) is indeed the catalytically competent

species. Further experimental studies as well as DFT calculations suggested that the amination of the allylic acetate intermediate proceeds by an $S_N1$ ligand exchange mechanism mediated by Cp*Rh(III) acting as a Lewis acid catalyst. We note that this study provides insights that are likely applicable to the related rhodium catalyzed allylic etherification and heteroarylation reactions that were recently disclosed,[8a, 8i] but likely do not explain the allylic arylation reaction utilizing aryl boronic acids,[8e] or the allylic amidation processes using dioxazolone reagents.[8b, 8d, 8f] Further studies to provide a unified mechanistic picture of this emergent field are required. These findings are of particular importance in the future design of regio– and enantioselective reactions as they clearly demonstrate that the critical C–N bond forming reaction does not occur via reductive elimination from the Rh-catalyst. Instead, processes that intercept the allylic acetate intermediate will need to be developed.

## ASSOCIATED CONTENT

### Supporting Information

The supporting information is available free of charge on the ACS Publications website at DOI:

Experimental procedures, computational details, x-ray crystal structure reports, and NMR spectra

### Author Information

#### Corresponding Author

*E-mail: mbaik2805@kaist.ac.kr

*E-mail: sblakey@emory.edu

### ORCID

Mu-Hyun Baik: 0000-0002-8832-8187

Simon B. Blakey: 0000-0002-4100-8610

Robert J. Harris: 0000-0003-0640-3487

Jiyong Park: 0000-0002-3225-4510

Taylor A. F. Nelson 0000-0002-4685-1455

Daniel C. Salgueiro 0000-0002-6162-3493

Cora E. MacBeth: 0000-0003-3877-2236

John Bacsa: 0000-0001-5681-4458

#### Notes

The authors declare no competing financial interest.

## ACKNOWLEDGMENT

The research was supported in part by the Institute for Basic Science (IBS-R010-A1) in Korea, the National Science Foundation (NSF) under the CCI Center for Selective C–H Functionalization (CHE-1700982), and the American Chemical Society Petroleum Research Fund (ACS-PRF-59563-ND1). NMR studies for this research were performed on instrumentation funded by the NSF (CHE-1531620). The X-ray analysis was done by the Emory X-ray Crystallography Facility using the Rigaku Synergy-S diffractometer, supported by the NSF (CHE-1626172). We gratefully acknowledge Dan Liu (Department of Chemistry, Emory University) for electrochemical assistance.

## REFERENCES

1. (a) Wang, N.-X.; Xing, Y.; Zhang, W., Advances in Transition-Metal-Catalyzed Direct sp3-Carbon–Hydrogen Bond Functionalization. *Synlett* **2015,** *26*, 2088-2098; (b) Yang, X.; Shan, G.; Wang, L.; Rao, Y., Recent advances in transition metal (Pd, Ni)-catalyzed C(sp 3 ) H bond activation with bidentate directing groups. *Tetrahedron Lett.* **2016,** *57*, 819-836; (c) Saint-Denis, T. G.; Zhu, R.-Y.; Chen, G.; Wu, Q.-F.; Yu, J.-Q., Enantioselective C(sp)–H bond activation by chiral transition metal catalysts. *Science* **2018,** *359*; (d) Chu, J. C. K.; Rovis, T., Complementary Strategies for Directed C(sp )-H Functionalization: A Comparison of Transition-Metal-Catalyzed Activation, Hydrogen Atom Transfer, and Carbene/Nitrene Transfer. *Angew. Chem. Int. Ed.* **2018,** *57*, 62-101.
2. Li, C.-J., Cross-Dehydrogenative Coupling (CDC): Exploring C−C Bond Formations beyond Functional Group Transformations. *Acc. Chem. Res.* **2009,** *42*, 335-344.
3. (a) Heumann, A.; Reglier, M.; Waegell, B., Oxidation with Palladium Salts - Stereospecific and Regiospecific Acetoxylation of 4-Vinylcyclohexene Derivatives. *Angew. Chem. Int. Ed. Engl.* **1982,** *21*, 366-367; (b) Mcmurry, J. E.; Kocovsky, P., A Method for the Palladium-Catalyzed Allylic Oxidation of Olefins. *Tetrahedron Lett.* **1984,** *25*, 4187-4190; (c) Backvall, J. E.; Hopkins, R. B.; Grennberg, H.; Mader, M. M.; Awasthi, A. K., Multistep Electron-Transfer in Palladium-Catalyzed Aerobic Oxidations Via a Metal Macrocycle Quinone System. *J. Am. Chem. Soc.* **1990,** *112*, 5160-5166; (d) Hansson, S.; Heumann, A.; Rein, T.; Akermark, B., Preparation of Allylic Acetates from Simple Alkenes by Palladium(Ii)-Catalyzed Acetoxylation. *J. Org. Chem.* **1990,** *55*, 975-984; (e) Liron, F.; Oble, J.; Lorion, M. M.; Poli, G., Direct Allylic Functionalization Through Pd-Catalyzed C-H Activation. *Eur. J. Org. Chem.* **2014**, 5863-5883; (f) Wang, R. H.; Luan, Y. X.; Ye, M. C., Transition Metal-Catalyzed Allylic C(sp(3))-H Functionalization via eta(3)-Allylmetal Intermediate. *Chin. J. Chem.* **2019,** *37*, 720-743; (g) Propylene. In *Kirk-Othmer Encyclopedia of Chemical Technology*.
4. Chen, M. S.; Whilte, M. C., A Sulfoxide-Promoted, Catalytic Method for the Regioselective Synthesis of Allylic Acetates from Monosubstituted Olefins via C−H Oxidation. *J. Am. Chem. Soc.* **2004,** *126*, 1346-1347.
5. (a) Young, A. J.; White, M. C., Catalytic Intermolecular Allylic C-H Alkylation. *J. Am. Chem. Soc.* **2008,** *130*, 14090-14091; (b) Reed, S. A.; White, M. C., Catalytic Intermolecular Linear Allylic C−H Amination via Heterobimetallic Catalysis. *J. Am. Chem. Soc.* **2008,** *130*, 3316-3318; (c) Reed, S. A.; Mazzotti, A. R.; White, M. C., A Catalytic, Brønsted Base Strategy for Intermolecular Allylic C−H Amination. *J. Am. Chem. Soc.* **2009,** *131*, 11701-11706; (d) Pattillo, C. C.; Strambeanu, I. I.; Calleja, P.; Vermeulen, N. A.; Mizuno, T.; White, M. C., Aerobic Linear Allylic C–H Amination: Overcoming Benzoquinone Inhibition. *J. Am. Chem. Soc.* **2016,** *138*, 1265-1272; (e) Ma, R.; White, M. C., C-H to C-N Cross-Coupling of Sulfonamides with Olefins. *J. Am. Chem. Soc.* **2018,** *140*, 3202-3205; (f) Fraunhoffer, K. J.; White, M. C., syn-1,2-Amino Alcohols via Diastereoselective Allylic C−H Amination. *J. Am. Chem. Soc.* **2007,** *129*, 7274-7276; (g) Chen, M. S.; Prabagaran, N.; Labenz, N. A.; White, M. C., Serial Ligand Catalysis: A Highly Selective Allylic C−H Oxidation. *J. Am. Chem. Soc.* **2005,** *127*, 6970-6971; (h) Campbell, A. N.; White, P. B.; Guzei, I. A.; Stahl, S. S., Allylic C−H Acetoxylation with a 4,5-Diazafluorenone-Ligated Palladium Catalyst: A Ligand-Based Strategy To Achieve Aerobic Catalytic Turnover. *J. Am. Chem. Soc.*

**2010,** *132*, 15116-15119; (i) Yin, G. Y.; Wu, Y. C.; Liu, G. S., Scope and Mechanism of Allylic C-H Amination of Terminal Alkenes by the Palladium/PhI(OPiv)(2) Catalyst System: Insights into the Effect of Naphthoquinone. *J. Am. Chem. Soc.* **2010,** *132*, 11978-11987.
6. Cochet, T.; Bellosta, V.; Roche, D.; Ortholand, J.-Y.; Greiner, A.; Cossy, J., Rhodium(iii)-catalyzed allylic C–H bond amination. Synthesis of cyclic amines from ω-unsaturated N-sulfonylamines. *Chem. Commun.* **2012,** *48*, 10745.
7. Burman, J. S.; Blakey, S. B., Regioselective Intermolecular Allylic C−H Amination of Disubstituted Olefins via Rhodium/π-Allyl Intermediates. *Angew. Chem. Int. Ed.* **2017,** *56*, 13666-13669.
8. (a) Lerchen, A.; Knecht, T.; Koy, M.; Ernst, J. B.; Bergander, K.; Daniliuc, C. G.; Glorius, F., Non-Directed Cross-Dehydrogenative (Hetero) arylation of Allylic C(sp(3))-H bonds enabled by C-H Activation. *Angew. Chem. Int. Ed.* **2018,** *57*, 15248-15252; (b) Burman, J. S.; Harris, R. J.; Farr, C. M. B.; Bacsa, J.; Blakey, S. B., Rh(III) and Ir(III)Cp* Complexes Provide Complementary Regioselectivity Profiles in Intermolecular Allylic C-H Amidation Reactions. *ACS. Catal.* **2019,** *9*, 5474-5479; (c) Kazerouni, A. M.; Nelson, T. A. F.; Chen, S. W.; Sharp, K. R.; Blakey, S. B., Regioselective Cp*Ir(III)-Catalyzed Allylic C-H Sulfamidation of Allylbenzene Derivatives. *J. Org. Chem.* **2019,** *84*, 13179-13185; (d) Knecht, T.; Mondal, S.; Ye, J. H.; Das, M.; Glorius, F., Intermolecular, Branch-Selective, and Redox-Neutral Cp*Ir-III-Catalyzed Allylic C-H Amidation. *Angew. Chem. Int. Ed.* **2019,** *58*, 7117-7121; (e) Knecht, T.; Pinkert, T.; Dalton, T.; Lerchen, A.; Glorius, F., Cp*Rh-III-Catalyzed Allyl Aryl Coupling of Olefins and Arylboron Reagents Enabled by C(sp(3))-H Activation. *ACS. Catal.* **2019,** *9*, 1253-1257; (f) Lei, H. H.; Rovis, T., Ir-Catalyzed Intermolecular Branch-Selective Allylic C-H Amidation of Unactivated Terminal Olefins. *J. Am. Chem. Soc.* **2019,** *141*, 2268-2273; (g) Liu, Y. Q.; Yang, Y. D.; Wang, C. X.; Wang, Z. S.; You, J. S., Rhodium(iii)-catalyzed regioselective oxidative annulation of anilines and allylbenzenes via C(sp(3))-H/C(sp(2))-H bond cleavage. *Chem. Comm.* **2019,** *55*, 1068-1071; (h) Sun, J. Q.; Wang, K.; Wang, P. Y.; Zheng, G. F.; Li, X. W., Rhodium(III)-Catalyzed Oxidative Allylic C-H Indolylation via Nucleophilic Cyclization. *Org. Lett.* **2019,** *21*, 4662-4666; (i) Nelson, T. A. F.; Blakey, S. B., Intermolecular Allylic C-H Etherification of Internal Olefins. *Angew. Chem. Int. Ed.* **2018,** *57*, 14911-14915.
9. (a) Leahy, D. K.; Evans, P. A., Rhodium(I)-Catalyzed Allylic Substitution Reactions and Their Applications to Target Directed Synthesis. *ChemInform* **2005,** *36*; (b) Evans, P. A.; Nelson, J. D., Conservation of Absolute Configuration in the Acyclic Rhodium-Catalyzed Allylic Alkylation Reaction: Evidence for an Enyl(σ–π) Organorhodium Intermediate. *J. Am. Chem. Soc.* **1998,** *120*, 5581-5582.
10. (a) Satoh, T.; Miura, M., Oxidative coupling of aromatic substrates with alkynes and alkenes under rhodium catalysis. *Chemistry* **2010,** *16*, 11212-11222; (b) *Issues in Chemistry and General Chemical Research: 2011 Edition*. ScholarlyEditions: 2012; p 6580.
11. (a) Vásquez-Céspedes, S.; Wang, X.; Glorius, F., Plausible Rh(V) Intermediates in Catalytic C–H Activation Reactions. *ACS Catal.* **2017,** *8*, 242-257; (b) Li, L.; Brennessel, W. W.; Jones, W. D., An Efficient Low-Temperature Route to Polycyclic Isoquinoline Salt Synthesis via C−H Activation with $[Cp^*MCl_2]_2$(M = Rh, Ir). *J. Am. Chem. Soc.* **2008,** *130*, 12414-12419.
12. Periana, R. A.; Bergman, R. G., Rapid intramolecular rearrangement of a hydrido(cyclopropyl)rhodium complex to a rhodacyclobutane. Independent synthesis of the metallacycle by addition of hydride to the central carbon atom of a cationic rhodium π-allyl complex. *J. Am. Chem. Soc.* **1984,** *106*, 7272-7273.
13. Wakefield, J. B.; Stryker, J. M., Metallacyclobutanes from kinetic nucleophilic addition to $\eta^3$-allyl ethylene complexes of iridium. Regioselectivity dependence on nucleophile and allyl orientation. *J. Am. Chem. Soc.* **1991,** *113*, 7057-7059.
14. Shibata, Y.; Kudo, E.; Sugiyama, H.; Uekusa, H.; Tanaka, K., Facile Generation and Isolation of π-Allyl Complexes from Aliphatic Alkenes and an Electron-Deficient Rh(III) Complex: Key Intermediates of Allylic C–H Functionalization. *Organometallics* **2016,** *35*, 1547-1552.
15. Shin, K.; Park, Y.; Baik, M.-H.; Chang, S., Iridium-catalysed arylation of C–H bonds enabled by oxidatively induced reductive elimination. *Nat. Chem.* **2017,** *10*, 218.
16. Simmons, E. M.; Hartwig, J. F., On the Interpretation of Deuterium Kinetic Isotope Effects in C?H Bond Functionalizations by Transition-Metal Complexes. *Angew. Chem. Int. Ed.* **2012,** *51*, 3066-3072.
17. (a) Song, L.; Trogler, W. C., $[(Co)_3(PPh_3)2OsAg(O_2CCF_3)]$ - a Model for an Intermediate on the Reaction Coordinate in Electron-Transfer. *Angew. Chem. Int. Ed. Engl.* **1992,** *31*, 770-772; (b) Connelly, N. G.; Geiger, W. E., Chemical redox agents for organometallic chemistry. *Chem. Rev.* **1996,** *96*, 877-910.
18. Dagar, A.; Guin, S.; Samanta, S., AgSbF6 -Catalyzed Tandem Reaction of 2-Alkynylanilines with Cyclic Enynones: Efficient access to 3-Furo[3,2-c ]chromenylindoles and Related Scaffolds. *Asian J. Org. Chem.* **2017,** *7*, 123-127.

TOC Figure

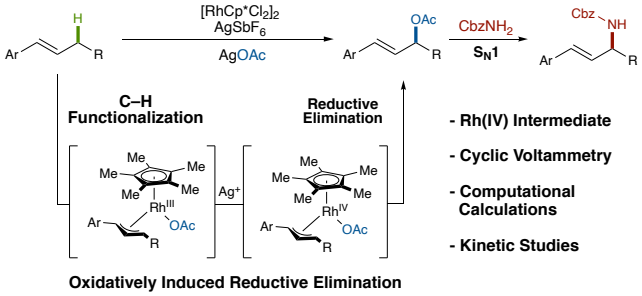
[RhCp*Cl2]2
AgSbF6
AgOAc
CbzNH2
SN1
C–H Functionalization
Reductive Elimination
- Rh(IV) Intermediate
- Cyclic Voltammetry
- Computational Calculations
- Kinetic Studies
Oxidatively Induced Reductive Elimination